ACS APPLIED MATERIALS & INTERFACES

Letter

www.acsami.org

Carbon Nanohorns As a High-Performance Carrier for MnO_2 Anode in Lithium-Ion Batteries

Heng Lai,[†] Jiaxin Li,[†,‡] Zhigao Chen,[†] and Zhigao Huang*[,†]

[†]College of Physics and Energy, Fujian Normal University, Fuzhou, 350007, China

[‡]Fujian Institute of Research on the Structure of Matter, Chinese Academy of Sciences, Fuzhou 350002, China

Supporting Information

ABSTRACT: MnO_2 nanoflakes coated on carbon nanohorns (CNHs) has been synthesized via a facile solution method and evaluated as anode for lithium-ion batteries. By using CNHs as buffer carrier, MnO_2/CNH composite displays an excellent capacity of 565 mA h/g measured at a high current density of 450 mA/g after 60 cylces.

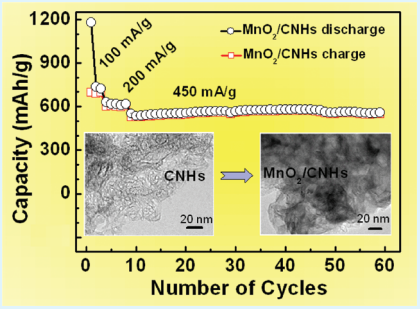

KEYWORDS: *MnO_2/CNH anode, buffer carrier, cycling performance, lithium-ion batteries*

Great efforts have been undertaken to increase the specific capacities of anode materials for high-power rechargeable lithium-ion batteries (LIBs).[1−3] Nanostructured transition metal oxides (MO_x) traditionally used as anode materials provide with multiple advantages for LIBs such as short path distance for Li ions and electron transport, intimate interaction between electrode and electrolyte, and good accommodation of the strain caused by electrochemical process.[3−7] Among various MO_x, manganese dioxides (MnO_2) have attracted great attention because of its high theoretical capacity of ∼1230 mA h/g[4] and relatively low electrochemical motivation force in comparison with other MO_x such as Fe_2O_3,[5] CoO_x,[6] and Cu_2O.[7] MnO_2 materials with various structures including nanowires,[8] nanotubes[9,10] and nanoflakes,[11] have been extensively developed for using as anodes in LIBs. However, the volume expansion, aggregation, and intrinsically low electronic conductivity during the cycling process commonly result in rapid fading of capacities for MnO_2 anodes. In practice, researchers mainly focused on using carbonaceous materials, such as carbon nanotubes[10,11] and graphene,[12] as buffer carriers for effectively suppressing the pulverization and capacity fading of MnO_2 anodes. Until recently, most reports can not achieved excellent cyclic stability and capacity for MnO_2 related anodes, especially stable cycling performance at higher current densities.

CNHs provided with good electric conductivity, large surface area as well as stable mechanical strength,[13−15] may effectively support MO_x anodes and improve their electrochemical performance in LIBs. Here, CNHs were used as buffer carrier for forming nanoflaky MnO_2/CNH composite for the first time. As a novel anode material, the reversible capacity of 565 mA h/g for MnO_2/CNHs (containing 42 wt % MnO_2) measured at 450 mA/g after 60 cycles can be obtained, which is much better than most of MnO_2 attached on other buffer carriers.

The general structure and morphology of CNHs, MnO_2, and MnO_2/CNH composite have been detected by XRD, SEM and TEM, respectively. Figure 1a shows the XRD patterns for CNHs, MnO_2 and MnO_2/CNH composite. Major peaks presented in MnO_2 and MnO_2/CNH composite can be indexed to the planes of MnO_2 crystal given by standard data file (JCPDS no. 80−1098). The strong peak of 26° observed in MnO_2/CNH pattern is coming from CNHs. To further investigate the oxidation state of Mn in the MnO_2/CNHs, we show the XPS result in Figure S1 (see the Supporting Information for details). The morphology of MnO_2 nanoflake can be seen from Figure 1b, which resembles the caterpillar aggregate.[11,16] TEM observed in Figure 1c shows a typical "dahlia-like" structure for CNHs. The TEM image shown in Figure 1d reveals MnO_2 layer enriched as "caterpillar" morphology, which is similar to the MnO_2 nanoflakes shown in Figure 1b. And the other SEM and TEM images for CNHs, and MnO_2, MnO_2/CNHs are shown in Figure S2 in the Supporting Information. In addition, the loading ratio of MnO_2 in MnO_2/CNH composite is 42 wt % based on TGA (see Figure S3 in the Supporting Information).

Figure 2 shows the cyclic voltammetry (CV) curves and the first two discharge−charge (D−C) profiles for CNHs, MnO_2, and MnO_2/CNH composite. The CV curves presented in Figure 2a clearly show the redox peaks are corresponding to the Li ions intercalate in or out CNHs reversibly.[15] The voltage

Received: March 1, 2012
Accepted: April 30, 2012
Published: April 30, 2012

   dx.doi.org/10.1021/am300378w | *ACS Appl. Mater. Interfaces* 2012, 4, 2325−2328

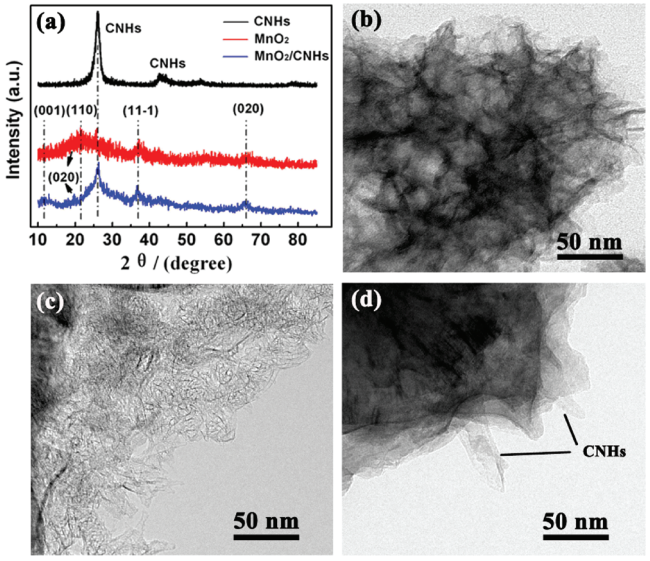

Figure 1. (a) X-ray diffraction patterns of the CNHs, MnO_2, and MnO_2/CNHs; (b) TEM image of MnO_2 nanoflakes; (c) TEM image of CNHs; (d) TEM image of MnO_2/CNHs.

plateaus for the first two D−C profiles of CNHs shown in Figure 2(d) are consistent with redox peaks of CV curves. For Figure 2b, the main cathodic peaks shown in the first cycle for MnO_2 are found at 2.60 and 0.55 V. The peak at 2.60 V is corresponding to the decomposed electrolyte. The 0.55 V at peak is assigned to the formation of a solid electrolyte interface (SEI) layer and the reduced reaction of MnO_2 with Li ions, which is described by $MnO_2 + 4\ Li^+ + 4\ e^- \rightarrow Mn\ (0) + 2\ Li_2O$.[10,11] Two oxidation peaks at 1.30 and 2.30 V in the first cycle can also be observed, which means that the electrochemical oxidation reaction may proceed by two steps. In the subsequent cycles, the 0.55 V reduction peak disappear, indicating that formation of the SEI layer only takes place during the first cycle. Compared to the CV curves of MnO_2 shown in Figure 2b, two oxidation peaks at 1.30 and 2.30 V presented in Figure 2c are more pronounced. It is observed from Figure 2c that the peaks in the following four cycles overlap well, indicating that a good electrochemical reversibility and structural stability for MnO_2/CNHs. Similarly, the related potential plateaus such as 1.30 and 2.30 V in the charge process for MnO_2/CNHs shown in Figure 2f, are more distinct than those of MnO_2 shown in Figure 2e. In addition, the discharge capacities for both MnO_2 and MnO_2/CNH electrodes are larger than the theoretical capacities, which may be attributed to the decomposition of electrolyte and the formation of SEI layer on the surface of the electrode.

The cycling performance for the electrodes of CNHs, MnO_2 and MnO_2/CNH composite in the voltage range of 0.05−3.0 V are displayed in Figure 3a−c. Figure 3a shows that CNH electrode delivered a specific reversible capacity of 215 mA h/g for CNHs after 60 cycles, indicating good cycling performance. However, the capacity for the MnO_2 electrode decreased obviously with the increasing cycle numbers. The specific

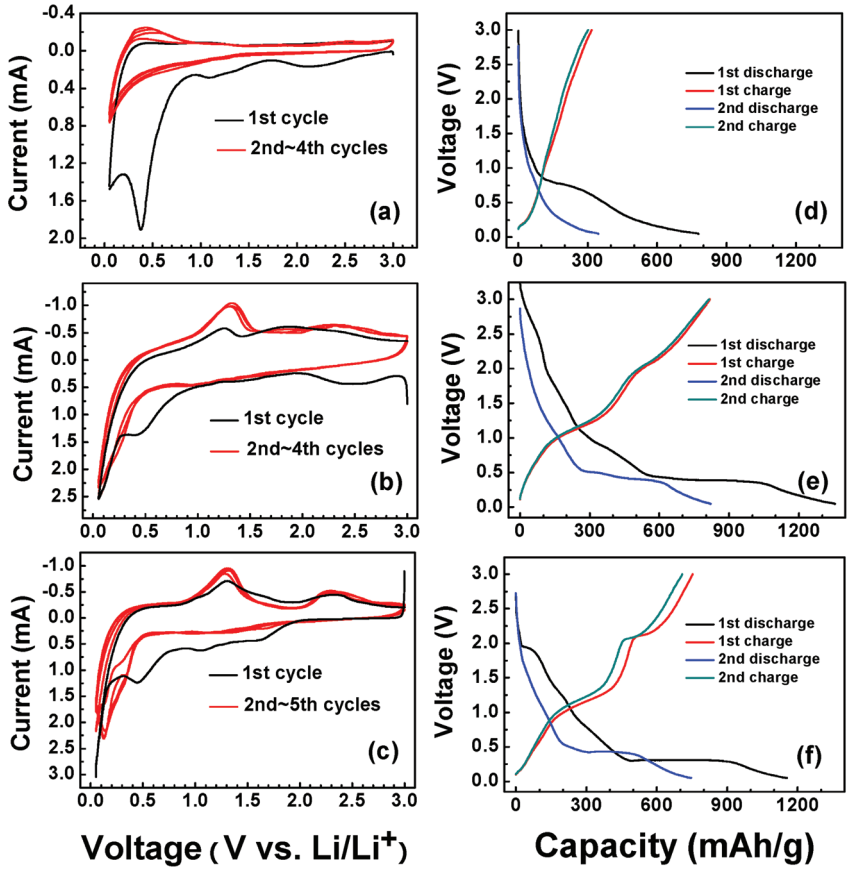

Figure 2. Cyclic voltammetry curves and first two discharge−charge curves between 0.05 and 3 V (versus Li/Li^+) of Li insertion/extraction into/from three kinds of electrodes: (a, d) CNHs, (b, e) MnO_2, and (c, f) MnO_2/CNHs.

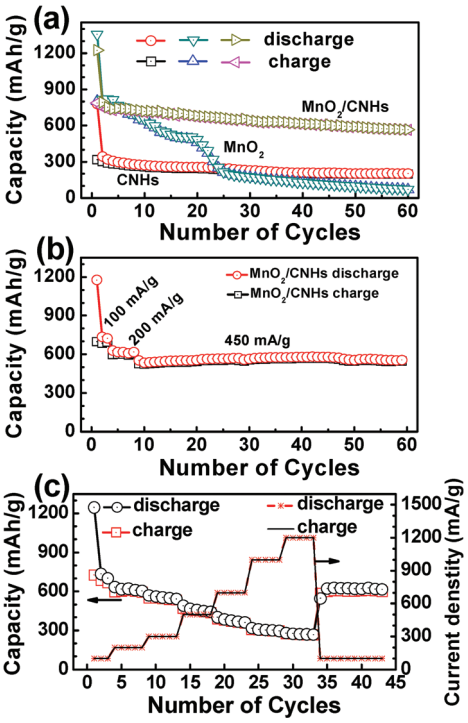

Figure 3. (a) Cycling performance of CNHs, MnO_2 and MnO_2/CNH electrodes at a current density of 100 mA/g; (b) cycling performance of MnO_2/CNH electrode at a current density of 450 mA/g; (c) capacity of MnO_2/CNH electrode at various current rates from 100 mA/g to 1200 mA/g with respect to the cycle number.

capacity of MnO_2 was only 100 mA h/g after 60 cycles. The severe capacity fading of MnO_2 electrode should be resulted from its aggregation and pulverization during electrochemical processes. The MnO_2/CNH composite tested at 100 mA/g presents the better electrochemical performance than that of MnO_2. Figure 3b shows that the specific reversible capacity stabilized at 565 mA h/g after 60 cycles, corresponding to a large capacity retention of 98%. In addition, the cycling performance of MnO_2/CNH composite tested at 300 and 1000 mA/g is shown in Figure S4 in the Supporting Information. The representative rate performance of the MnO_2/CNH composite is shown in Figure 3c. The fairly stable capacities at different current densities can be observed, even at a high rate of 1200 mA/g. When the cycling current was reduced back to 100 mA/g, the electrode can still deliver a reversible capacity of 620 mA h/g, implying that the structure of the electrode remained stable after various rate cycles.

Subtracting the contribution from CNHs in MnO_2/CNH composite, a reversible capacity of 1180 mA h/g can be attributed to MnO_2, indicating 96% of the theoretical capacity of MnO_2 (1230 mA h/g). By measuring at 100 mA/g, the capacity of 1180 mA h/g and the ratio of 96% can be calculated by the following equations: $[C_{MnO_2/CNHs} - (C_{CNHs}\cdot 58\ wt\ \%)]/42\ wt\ \% = [620 - (215\cdot 0.58)]/0.42 = 1180$ and $1180/1230 = 96\%$. Thus, the reversible capacity of MnO_2 loading on CNHs can almost achieve its theoretical capacity under low current densities in this current study. It is concluded that the electrochemical performance of MnO_2/CNH composite can be strongly improved by using CNHs as buffer carrier. According to the EIS result shown in Figure S5 in the Supporting Information, the excellent performance of MnO_2/CNH composite is ascribed to the good conductivity and electronic contact between MnO_2 and CNH buffer carrier. These electrochemical properties based on the overall mass of the MnO_2/CNH composite are comparable with the latest results on MnO_2 loading on other carbon buffer carriers.[10,12] Furthermore, other carbon-based material such as multiwalled carbon nanotubes (MWNTs) have been also used as carrier for loading MnO_2 and investigated as anode for LIBs. The experiment details have been shown in the Supporting Information.The electrochemical performance is shown in Figures S6−S9 in the Supporting Information. To further compare the electrochemical performance of the typical MnO_2-related anodes based on different carbon carrier materials, some relevant information are summarized in Table S1 in the Supporting Information. Especially, the stabilities of cycling performance at high current densities are much better than most of previous reports. The excellent electrochemical performance of the MnO_2 coated on CNHs buffer carrier can be attributed to the following reasons. Combination of CNHs could increase electronic conductivity of the composite and hamper the aggregation of MnO_2 during discharge and charge progress. Furthermore, the high surface area of CNHs and the uniform distribution of MnO_2 might provide a fine electrode/electrolyte contact area and short path length for Li^+ transport, thus improving the stability of discharge capacity of the MnO_2/CNHs composite.[15]

In summary, CNHs were used as buffer carrier for synthesizing nanoflaky MnO_2/CNH composite via a simple solution method for the first time. As a novel anode material, the MnO_2/CNH composite exhibits excellent electrochemical properties with long-cycling capacity and high-rate performance. The large capacity of 565 mA h/g for this MnO_2/CNH composite even measured at a high current density of 450 mA/g after 60 cycle can be obtained, revealing that the nanoflaky MnO_2/CNH composite could be a promising anode material for LIBs.

■ ASSOCIATED CONTENT

Ⓢ Supporting Information

Experimental details; XPS, TEM, SEM, and TGA of composites (Figures S1−S3); electrochemical performance results of MnO_2/CNH s and MnO_2/MWNTs (Figures S4−S9, Table S1). This material is available free of charge via the Internet at http://pubs.acs.org/.

■ AUTHOR INFORMATION

Corresponding Author

*Telephone/Fax: 86-591-22867577. E-mail: zghuang@fjnu.edu.cn.

Notes

The authors declare no competing financial interest.

■ ACKNOWLEDGMENTS

We gratefully acknowledge the financial support by the Natural Science Foundation of China (11074039) and the National Key Project for Basic Research of China (2011CBA-00200) .

■ REFERENCES

(1) Armand, M.; Tarascon, J. M. *Nature* **2008**, *451*, 652.
(2) Sun, Y.; Wu, Q.; Shi, G. *Energy Environ. Sci.* **2011**, *4*, 1113.
(3) Cheng, F.; Tao, Z.; Liang, J.; Chen, J. *Chem. Mater.* **2007**, *20*, 667.
(4) Fang, X.; Lu, X.; Guo, X.; Mao, Y.; Hu, Y.S. J.; Wang, Z.; Wang, F.; Wu, H.; Liu, L.; Chen. *Electrochem. Commun.* **2010**, *12*, 1520.
(5) Wu, M. S.; Ou, Y. H.; Lin, Y. P. *Electrochim. Acta* **2010**, *55*, 3240.

(6) Nam, K. M.; Shim, J. H.; Han, D. W.; Kwon, H. S.; Kang, Y. M.; Li, Y.; Song, H.; Seo, W. S.; Park, J. T. *Chem. Mater.* **2010**, *22*, 4446.
(7) Xiang, J. Y.; Tu, J. P.; Yuan, Y. F.; Huang, X. H.; Zhou, Y.; Zhang, L. *Electrochem. Commun.* **2009**, *11*, 262.
(8) Wu, M. S.; Chiang, P. C.; Lee, J. T.; Lin, J. C. *J Phys Chem B* **2005**, *109*, 23279.
(9) Yu, A.; Park, H. W.; Davies, A.; et al. *J. Phys. Chem. Lett.* **2011**, *2*, 1855.
(10) Reddy, A. L. M.; Shaijumon, M. M.; Gowda, S. R.; Ajayan, P. M. *Nano Lett.* **2009**, *9*, 1002.
(11) Xia, H.; Lai, M.; Lu, L. *J. Mater. Chem.* **2010**, *20*, 6896.
(12) Xing, L.; Cui, C.; Ma, C.; Xue, X. *Mater. Lett.* **2011**, *65*, 2104.
(13) Tu, W.; Lei, J.; Ding, L.; Ju, H. *Chem. Comun.* **2009**, 4227.
(14) Cioffi, C.; Campidelli, S.; Sooambar, C.; et al. *J. Am. Chem. Soc.* **2007**, *129*, 3938.
(15) Zhao, Y.; Li, J.; Ding, Y.; Guan, L. *Chem. Commun.* **2011**, *47*, 7416.
(16) Li, J.; Wang, N.; Zhao, Y.; Ding, Y.; Guan, L. *Electrochem. Commun.* **2011**, *13*, 698.